Short communication

A novel direct methanol fuel cell with sol–gel flux phase

Jianfeng Ju*, Donghui Wu, Cunwang Ge, Yujun Shi*

School of Chemistry and Chemical Engineering, Nantong University, Nantong 226007, Jiangsu, PR China

ABSTRACT

The sol–gel flux phase of direct methanol fuel cell is prepared by the modified sol–gel method with starting materials of Na_2SiO_3 or $Si(OCH_3)_4$, methanol and sulfuric acid, and characterized by SEM. The methanol permeability and electrochemical characteristics of the sol–gel flux phase are investigated. The mass transportation mechanism and the process of methanol has been changed by the porous structure of the sol–gel flux phase. The methanol permeability of the sol–gel flux phase decreases more than 90% compared with the liquid flux phase of $1\,mol\,L^{-1}\,CH_3OH$ and $1\,mol\,L^{-1}\,H_2SO_4$. A novel direct methanol fuel cell with sol–gel flux phase is designed. The power density of which is higher than that of the cell with liquid flux phase.

© 2009 Elsevier B.V. All rights reserved.

1. Introduction

The direct methanol fuel cell (DMFC) is one of the most promising portable power sources for mobile electronic devices (e.g., laptops, cellular phones and PDAs). The advantages of DMFCs are reasonably high specific energy, convenient storage of fuel, and low temperature operation [1,2]. Nevertheless, several problems and technological issues still remain, such as methanol crossover, high catalyst loading and low power density [3–5], which will significantly reduce the overall efficiency of the fuel cell system. A fraction of methanol fuel at the anode is transported to the cathode due to the concentration gradient, which reacts directly with the oxygen at the cathode, and no current is produced. Additionally, the catalytic activity together with the performance of the cell declines due to its toxicity [6].

Admixture of methanol and H_2SO_4 is commonly used as flux phase of DMFC. The transportation and permeability of methanol influence the performance of DMFC. Recently, there has been considerable interest in the research of the flux phase which include methanol permeability and mass transportation of flux phase to the proton exchange membrane, mass transportation model, proton exchange membrane of lower leakage and the catalysts of higher tolerance to CO [7–10]. Although these studies have made headway, none of them can solve the problem of methanol permeability. To our knowledge, there are fewer reports to increase the performance of DMFC by means of improving the of flux phase to solve the problem of methanol permeability. Amir and Zhen [11] developed a new protocol to reduce the methanol permeability by designing

the configuration of DMFC that change the feed of methanol from liquid phase to vapor. On the third international hydrogen fuel cell exhibition, Japanese SINANEN exhibited a DMFC system using solid methanol as fuel, which reduces the methanol permeability of the flux phase using solid methanol as fuel. But it is much dear to produce solid methanol, and the mass transportation is limited so as to influence the process of anodic reaction.

In this paper, we developed a method to restrain the methanol permeability with sol–gel flux phase of DMFC. The sol–gel flux phase is prepared by the modified sol–gel method, which is composed of dispersion medium and the gelatinizer, the former composes of methanol and sulfuric acid, while SiO_2 is used as the latter. The methanol permeability and electrochemical characteristics of the sol–gel flux phase together with the form of the flux phase and mass transportation mechanism of methanol have been investigated. The mass transportation mechanism and the process of methanol has been changed by the porous structure of the sol–gel flux phase. The methanol permeability of the sol–gel flux phase decreases more than 90% compared with the liquid flux phase of $1\,mol\,L^{-1}\,CH_3OH$ and $1\,mol\,L^{-1}\,H_2SO_4$. A novel DMFC with sol–gel flux phase is designed, and the density of the DMFC with sol–gel flux phase and liquid flux phase of $1\,mol\,L^{-1}\,CH_3OH$ and $1\,mol\,L^{-1}\,H_2SO_4$ has been determined at $60\,°C$, respectively.

2. Experiments and the novel direct methanol fuel cell design

2.1. Synthesis of the sol–gel flux phase

The sol–gel flux phase was prepared by the modified sol–gel method. Na_2SiO_3 or $Si(OCH_3)_4$ (according to the massfraction of SiO_2 5% that formed in the sol–gel flux phase) was weighed, and

---

* Corresponding authors. Tel.: +86 513 85015496; fax: +86 513 85015501.
E-mail addresses: jjf1969@163.com (J. Ju), yujunshi2001@163.com (Y. Shi).

dissolved in deionized water, after that, the calculated H_2SO_4, methanol, and Sodium alginate (aqueous solution of 0.5% mass-fraction) was dropped under stirring. The mixture in the glass was airproofed and continually stirred. Na_2SiO_3 or $Si(OCH_3)_4$ hydrolyzed slowly to form the sol eventually. The viscidity of the system was increased with the proceeding of hydrolysis reaction. Finally, the semisolid humid gel was formed with methanol aqueous solution as dispersion medium at the concentration of methanol and H_2SO_4 of $1 \, mol \, L^{-1}$, which was denoted the sol–gel flux phase.

2.2. Sol–gel flux phase methanol permeability

A diaphragm diffusion cell, as described in detail elsewhere [12,13], was used to determine the methanol permeability of the sol–gel flux phase. The apparatus consists of plastic compartments (A and B), which were separated by the Nafion 117 membrane with an effective area of $4.09 \, cm^2$ and thickness of 1 mm. The compartment A (volume $100 \, cm^3$) was filled with the sol–gel flux phase while the compartment B (volume $100 \, cm^3$) was filled with distilled water. The methanol molecules diffuse along the concentration gradient through the Nafion 117 membrane into the opposite compartment of the diffusion cell. Magnetic stirrer was used in each reservoir to ensure uniformity during the diffusion experiment. Prior to determination, Nafion 117 membrane was dipped in the solution of 70% H_2SO_4 and 30% H_2O_2 over 24 h. To determine the methanol permeability of Nafion 117 membrane, liquid samples of $10 \, \mu L$ were drawn hourly from the permeate compartment using a syringe and the samples were then analyzed with a gas chromatography (Ruihong Chemical Engineering Instrument Co., Ltd., Shandong). Methanol diffusion is induced by a concentration gradient across the membrane. Hence, from the change of methanol concentration in the diffusion reservoir, the diffusion coefficient is obtained by the following equation.

The methanol concentration in diffusion reservoir (C_B) at time t was calculated from the linear interpolation of C_B versus t and the slope (σ) of the graph can be written as follows:

$$\sigma = \frac{\Delta C}{\Delta t}$$

$$C_B = \sigma t$$

where the C_B is the concentration of methanol in diffusion reservoir ($mol \, L^{-1}$) at time t, t is diffusion time, ΔC is the variable concentration of methanol, Δt is dispersion time 1 h.

The permeability of methanol ($cm^2 \, s^{-1}$) was expressed as below:

$$P = \sigma \frac{V_B L}{A C_A}$$

where C_A is the concentration of methanol in feed compartment ($mol \, L^{-1}$), A is the effective area of membrane (cm^2), L is the membrane thickness (cm), and V_B is the volume of diffusion reservoir (cm^3).

2.3. Electrochemical measurement of sol–gel flux phase

The electrochemical measurements were performed on CHI 660C workstation (American CHI Instrument). The electrochemical cell consisted of a tri-electrode system with platinum wire as counter, a saturated calomel electrode (SCE) as reference, and a modified carbon paste electrode (CPE) as working electrode, respectively. The anode catalyst of $PtRu/TiO_2-SiO_2/C$ was prepared according to the method of Chinese patent [14]. The preparation of carbon paste electrode was prepared according to a previous report [15]. Typically, the anode catalyst of 5 mg was mixed completely
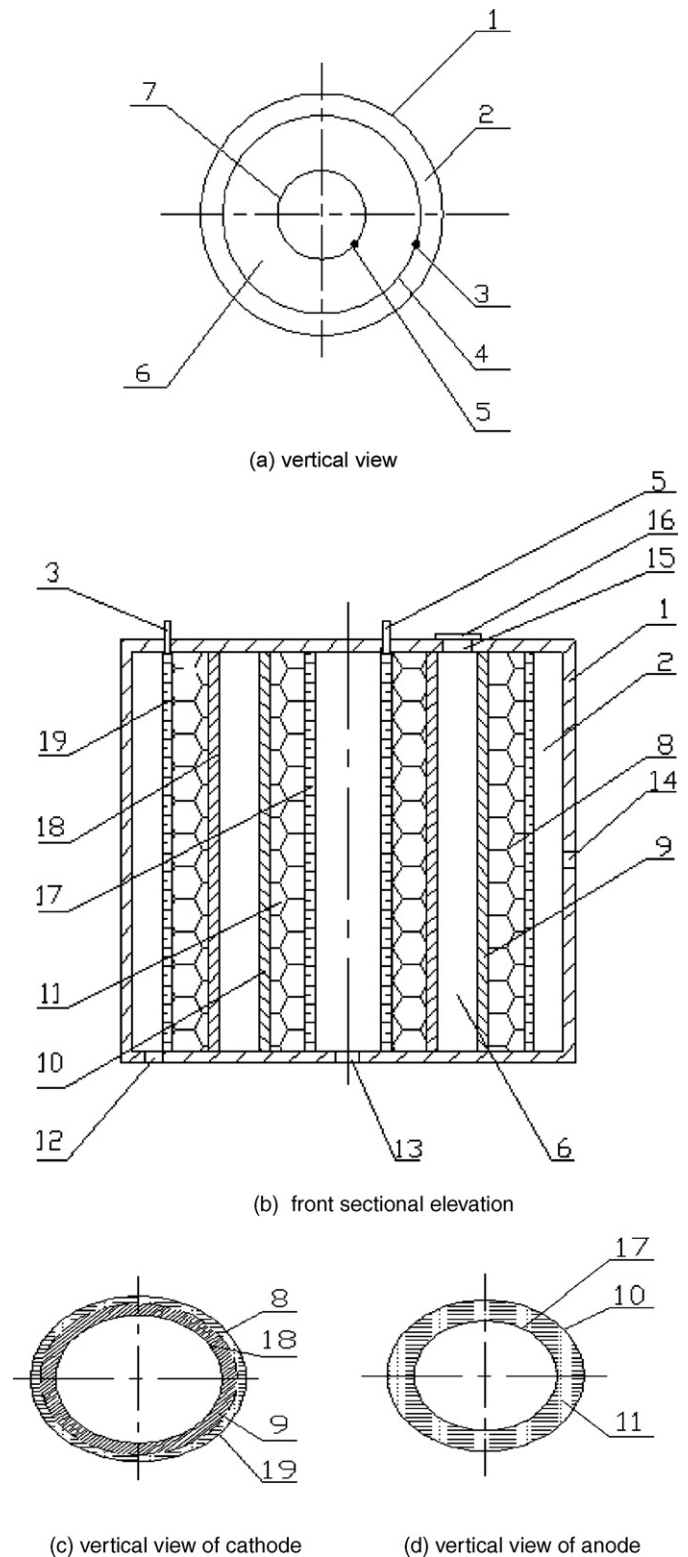

(a) vertical view

(b) front sectional elevation

(c) vertical view of cathode   (d) vertical view of anode

Fig. 1. Diagram of the membraneless using sol–gel flux phase. (a) Vertical view; (b) front sectional elevation; (c) vertical view of cathode; (d) vertical view of anode. Novel direct fuel cell architecture: 1, shell; 2, air room; 3, cathode output contact; 4, cathode; 5, anode output contact; 6, sol–gel flux phase room; 7, anode; 8, diffuse layer; 9, cathode catalyst; 10, anode catalyst; 11, diffuse layer; 12, water-drain hole; 13, CO_2-drain hole; 14, ventilation hole; 15, feed fuel hole; 16, feed fuel sealing head; 17, porous titanium plate; 18, Nafion membrane; 19, porous titanium plate.
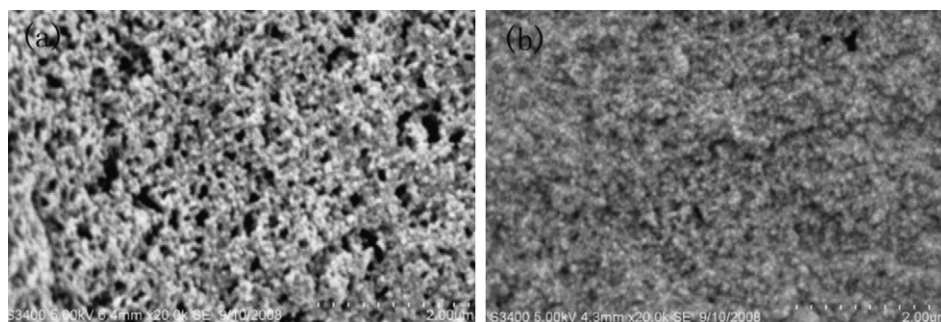
Fig. 2. SEM photographs of the sol–gel flux phase. (a) Na_2SiO_3 as material and (b) $Si(OC_2H_5)_4$ as material.

with paraffin of 30 μL and some VulcanXC-72 in the evaporating dish, followed by evaporation of the water under vacuum. The mixture was finally packed into an electrode cavity of Teflon (3-mm diameter, 5-mm depth). Electrical contact to the paste was established by forcing a copper rod into the back of the mixture. After being polished manually on a weighing paper, the modified electrode was used as the working electrode. The electrolyte was liquid flux phase or sol–gel flux phase of $1\,mol\,L^{-1}$ H_2SO_4 and $1\,mol\,L^{-1}$ methanol. The electrochemical performance was carried at room temperature with the purge of N_2.

2.4. Scanning electron microscope

The morphology of the sol–gel flux phase was investigated using scanning electron microscope (SEM, Hitachi Japan). Specimen for the SEM was prepared by freezing the sol–gel flux phase sample in liquid nitrogen up to 10 min and breaking it to produce a cross-section (Hitachi Japan). Fresh cross-sectional cryogenic fractures of the sol–gel flux phase was sputtered with a thin layer of Pt with an ion sputtering in vacuum before viewing.

2.5. Novel direct methanol fuel cell design

The design of the fuel cell assembly was shown in Fig. 1.

The novel direct fuel cell is circular architecture, the anode consists of three layers, the porous titanium plate or stainless steel plate form the inner layer, anode catalyst (Pt–Ru, $4\,mg\,cm^{-2}$) form the out layer, while the diffusion layer composes of carbon fiber paper or carbon fiber cloth. So does the cathode, with a bit difference of out layer, in which Pt of $4\,mg\,cm^{-2}$ acts as catalyst (covered with Nafion 117 membrane). The electrode area is $4\,cm^2$, and the volume of the sol–gel flux phase is $10\,cm^3$.
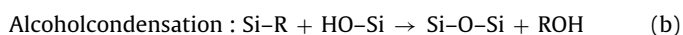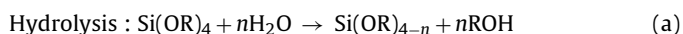
3. Results and discussion

3.1. Sol–gel flux phase characterization

The SEM photographs of the sol–gel flux phase using Na_2SiO_3 and $Si(OCH_3)_4$ as starting materials were presented in Fig. 2.

Both of the sol–gel flux phases had porous structure with the bone of SiO_2. SiO_2 was well distributed in the medium of methanol and water. From Fig. 2(a), we can see that the aperture of the sol–gel flux phase using Na_2SiO_3 as material is ranging from 50 nm to 60 nm. It is much bigger than that of 20 nm with $Si(OCH_3)_4$ as starting materials in Fig. 2(b). It is probably attributed to the preparation mechanism of the sol–gel flux phase.
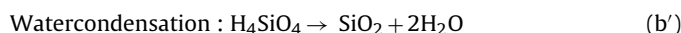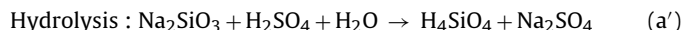
The formation of as-prepared silica sol–gel using $Si(OCH_3)_4$ as material typically undergo three elementary reactions [16]:

$$\text{Hydrolysis}: Si(OR)_4 + nH_2O \rightarrow Si(OR)_{4-n} + nROH \qquad (a)$$

$$\text{Alcoholcondensation}: Si-R + HO-Si \rightarrow Si-O-Si + ROH \qquad (b)$$

$$\text{Watercondensation}: Si-OH + HO-Si \rightarrow Si-O-Si + H_2O \qquad (c)$$

It is important to note that only the condensation reactions are responsible of the gel formation. The hydrolysis rate of the route using $Si(OCH_3)_4$ as material was greatly influenced by water than that of Na_2SiO_3.

The pH dependence of this set of reactions has been extensively studied [16–19]. The hydrolysis rate reaches the minimum at neutral pH and almost rises when the pH is lowered or increased. The condensation rate, on the contrary, is the highest at neutral pH and sharply decreases far from neutrality, the condensation rate rises sharply when the pH is small than 3. The relation among the gelatinizing time and pH is presented "N" curve [17,18].

The formation of as-prepared silica sol–gel using Na_2SiO_3 as material undergo two elementary reactions:

$$\text{Hydrolysis}: Na_2SiO_3 + H_2SO_4 + H_2O \rightarrow H_4SiO_4 + Na_2SO_4 \qquad (a')$$

$$\text{Watercondensation}: H_4SiO_4 \rightarrow SiO_2 + 2H_2O \qquad (b')$$

The hydrolysis rate reaches the minimum at neutral pH and almost rises when the pH is lowered or increased. The condensation rate, on the contrary, is highest at neutral pH and sharply decreases far from neutrality. The relation among the gelatinizing time and pH is presented "V" curve [16,20].

Often an alcohol is employed for rendering the system homogeneous, the addition of methanol decrease the hydrolysis rate to some extent. The reaction system contains only 5 wt% silica and $1\,mol\,L^{-1}$ of methanol, the effect of the addition of methanol on the gelatinizing time is smaller.

The concentration of H_2SO_4 in the solution is $1\,mol\,L^{-1}$, the gelatinizing time of the sol–gel flux phase using material of $Si(OCH_3)_4$ should be shorter than that of Na_2SiO_3.

The aperture was influenced by the formation rate of the sol–gel flux phase. The more the formation rate of the sol–gel flux phase was, the smaller aperture would be in the aqueous medium for dispersing. Its aperture is smaller than 20 nm [20]. The experiments result show that the gelatinizing time using Na_2SiO_3 as material is more than 20 days, its aperture is about 50–60 nm. While, the gelatinizing time using $Si(OCH_3)_4$ as material is about 2 days, its aperture is 20 nm. Both of the apertures of the sol–gel flux phase were bigger than 20 nm. This is probably because of the dispersing medium is methanol except water.

3.2. Methanol permeability performance of the sol–gel flux phase

Fig. 3 shows temporal dependence of the methanol permeability concentration of the sol–gel flux phase.

The methanol permeability of the sol–gel flux phase using material of Na_2SiO_3 and $Si(OCH_3)_4$ were calculated from Fig. 3 with the results of $1.26 \times 10^{-7}\,cm^2\,s^{-1}$ and $8.15 \times 10^{-8}\,cm^2\,s^{-1}$, respectively. Both of them were decreased more than 90% com-

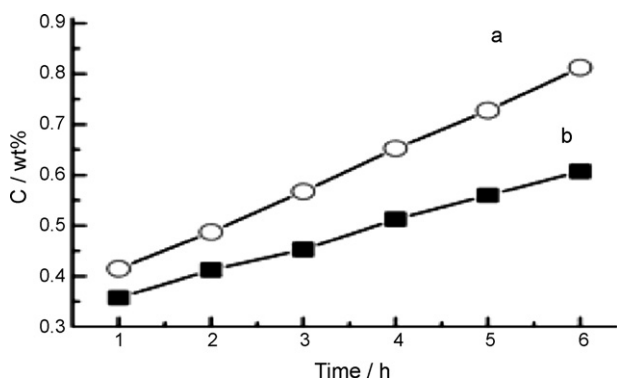**Fig. 3.** Temporal dependence of the methanol permeability concentration of the sol–gel flux phase. (a) Na_2SiO_3 as material and (b) $Si(OC_2H_5)_4$ as material.

pared with that of the liquid flux phase of $1\,mol\,L^{-1}$ methanol and $1\,mol\,L^{-1}$ H_2SO_4 to Nafion 117 membrane [12]. This indicated that the methanol permeability of sol–gel flux phase is far lower than that of the liquid flux phase.

The mass transportation of mechanism and process of methanol can be changed by the porous structure of the sol–gel flux phase. The methanol permeability in the liquid flux phase mainly expresses the permeation of the methanol over the surface of Nafion membrane. Although the sol–gel flux phase contact closely with the Nafion membrane, the sol–gel flux phase is the half-flux phase without fluidity, methanol expresses only the diffusion over the Nafion membrane. Before its diffusion over Nafion membrane, it exists mass transport resistance of methanol from the sol–gel flux phase to interface. Compared with the permeating, the diffusing rate of methanol is slower. Accordingly, the sol–gel flux phase can reduce the methanol permeability over the Nafion membrane.

The methanol permeability of the sol–gel flux phase prepared with Na_2SiO_3 is a little higher than that with $Si(OCH_3)_4$. This is probably due to the fact that the mass transportation of methanol in the sol–gel flux phase takes place from the bore to the interface, besides the diffusion through the Nafion membrane. Because of the bore diameter of the sol–gel flux phase prepared with Na_2SiO_3 is bigger than with $Si(OCH_3)_4$, the mass transport resistance of methanol diffusion from the sol–gel flux phase to the interface is smaller, the concentration of methanol diffuses through the Nafion membrane becomes a little higher over, the methanol permeability is a little higher.

3.3. Electrochemical performance of the sol–gel flux phase

The cyclic voltammograms of $PtRu/TiO_2$–SiO_2/C in sol–gel flux phase with starting material of $Si(OCH_3)_4$ and liquid flux phase are shown in Fig. 4.

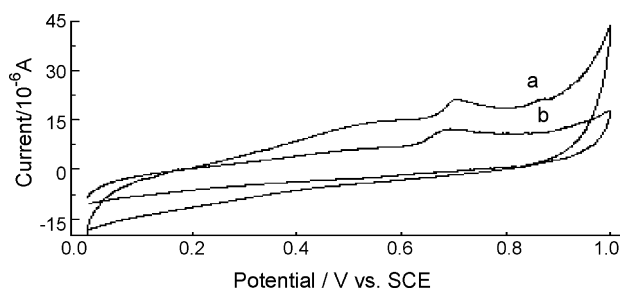The potential of oxidation peak of the sol–gel flux phase is 0.707 V with oxidation peak current 5.499×10^{-6} A while the

Fig. 4. Cyclic voltammograms of $PtRu/TiO_2$–SiO_2/C in sol–gel flux phase (a) and liquid flux phase (b).
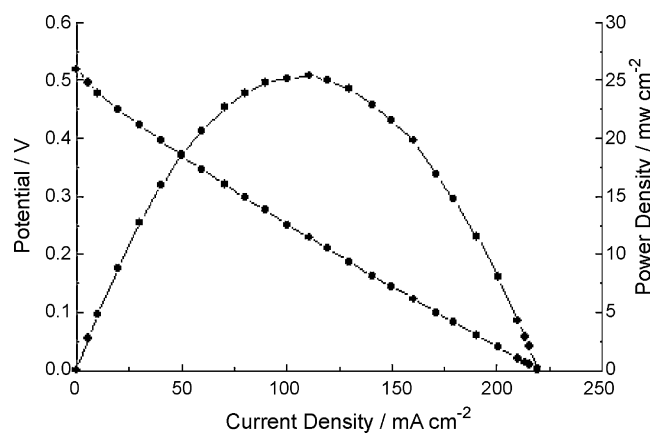

Fig. 5. Characteristic curves of the novel DMFC using the sol–gel flux phase.

potential of oxidation peak of the liquid flux phase was 0.693 V with oxidation peak current 4.817×10^{-6} A. Compared with the liquid flux phase, the potential and current of oxidation peak of sol–gel flux phase was bigger. As reported in the literature [21], the current increases as the concentration of methanol aggrandizes, the active oxygen absorbed on the surface of catalyst decreases with the rise of methanol concentration, it is needed to form much more active oxygen under higher potential, meanwhile, the oxidation peak current increases. According to Fig. 3 and the results in the literature [21], methanol concentration of the sol–gel flux phase absorbed on the surface of catalyst was a little higher than that of the liquid flux phase.

Methanol dispersed uniformly in the sol–gel flux phase, the mass transportation of methanol expressed not only by the diffusion but also the bore of the sol–gel flux phase, and form the gradient of methanol compared with the liquid flux phase, the sol–gel flux phase is apt to the mass transportation of methanol to the surface of catalyst.

3.4. DMFC characterization

The I–V characteristic curves of the DMFC were obtained by operating them at different condition with CHI660. Figs. 5 and 6 show the obtained results for the potential and the power density versus the current density for the sol–gel flux phase with starting material of $Si(OCH_3)_4$ and liquid flux phase.

Compared with the maximum power density $16.2\,mW\,cm^{-2}$ of the DMFC using the liquid flux phase, the maximum power density of the DMFC using the sol–gel flux phase is around $25.4\,mW\,cm^{-2}$. The power density of the latter is 50% larger than that of the anterior. The key factor to understand the behavior difference in a DMFC under different flux phase is the crossover effect. This effect is due to the crossing over of methanol from the anode to the cathode
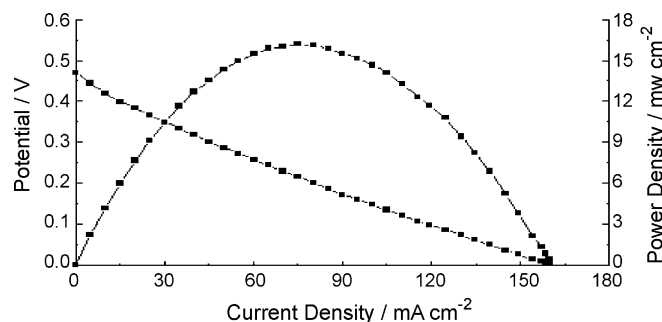

Fig. 6. Characteristic curves of the novel DMFC using the liquid flux phase.

through the Nafion 117 membrane. This results not only in a fuel loss, but also in a decrease in the overall cell voltage due to the mixed potential on the cathode. The explanation of the behavior difference observed in our DMFC when it is operated with the liquid flux phase and sol–gel flux phase comes from the effect of the crossover in the performance of the DMFC. The methanol permeability of the sol–gel flux phase is decreased more than 90% compared with that of the liquid flux phase of $1\,mol\,L^{-1}$ methanol and $1\,mol\,L^{-1}$ H_2SO_4 to Nafion 117 membrane. This is the key factor to effect the power density of the DMFC. The results indicate that the mass transportation of methanol from the flux phase to the surface of anode is not influenced by the sol–gel flux phase or liquid flux phase.

4. Conclusions

We have prepared the sol–gel flux phase of DMFC to solve the methanol permeability problem successfully. The sol–gel flux phase has porous structure that changes the mass transportation mechanism and process of methanol. The methanol permeability of the sol–gel flux phase decreased more than 90% compared with the liquid flux phase of $1\,mol\,L^{-1}$ CH_3OH and H_2SO_4. We designed a novel DMFC with the sol–gel flux phase. The maximum power density of the DMFC with sol–gel flux phase is higher than that with liquid flux phase. The flux phase is the key factor to affect the maximum power density of the DMFC.

Acknowledgements

References

[1] M. Baldauf, W. Preidel, Journal of Power Sources 84 (1999) 161–166.
[2] S. Wasmus, A. Kuver, Journal of Electroanalytical Chemistry 461 (1999) 14–31.
[3] A. Heinzel, V.M. Barragan, Journal of Power Sources 84 (1999) 70–74.
[4] J. Cruickshank, K. Scott, Journal of Power Sources 70 (1998) 40–47.
[5] X. Ren, P. Zelenay, S. Thomas, J. Davey, S. Gottesfeld, Journal of Power Sources 86 (2000) 111–116.
[6] Y.H. Chan, T.S. Zhao, R. Chen, C. Xu, Journal of Power Sources 178 (2008) 118–124.
[7] S. Shanumgam, B. Viswanathan, T.K. Varadarajan, Journal of Membrane Science 275 (1–2) (2006) 105–109.
[8] Z.M. Wu, G.Q. Sun, W. Jin, H.Y. Hou, S.L. Wang, Journal of Membrane Science 325 (1) (2008) 376–382.
[9] K.M. Yin, Journal of Power Sources 179 (2) (2008) 700–710.
[10] A. Bauer, E.L. Gyenge, C.W. Oloman, Journal of Power Sources 167 (2) (2007) 281–287.
[11] F. Amir, G. Zhen, Applied Thermal Engineering 28 (13) (2008) 1614–1622.
[12] M.N.A. Mohd Norddin, A.F. Ismail, D. Rana, T. Matsuura, A. Mustafa, A. Tabe-Mohammadi, Journal of Membrane Science 323 (2) (2008) 404–413.
[13] M.M. Nasef, N.A. Zubir, A.F. Ismail, K.Z.M. Dahlan, H. Saidi, M. Khayet, Journal of Power Sources 156 (2) (2006) 200–210.
[14] J.F. Ju, D.H. Wu, P. Hua, Y.J. Shi, Z.F. Xu, J.H. Li, G.J. Su, Q. Zhang, A kind of anode catalyst of direct methanol fuel cell and its preparation, Chinese Patent, CN10123912 (2008).
[15] C.W. Ge, M. Xu, J.H. Fang, J.P. Lei, H.X. Ju, Journal of Physical Chemistry 112 (2008) 10602–10608.
[16] F. Cellesi, N. Tirelli, Colloids and Surfaces A: Physicochemical and Engineering Aspects 288 (2006) 52–61.
[17] C.J. Brinker, Journal of Non-Crystalline Solids 100 (1988) 31–50.
[18] J. Sefcik, A.V. Mccormick, Journal of Physical Chemistry 96 (1992) 8973–8979.
[19] C.J. Brinker, Sol–gel Science, The Physics and Chemistry of Sol–Gel Processing, Academic Press Inc., London, 1990.
[20] T. Jesionowski, Materials Chemistry and Physics 113 (2009) 839–849.
[21] A.C.C. Tseung, P.K. Shen, K.Y. Chen, Journal of Power Sources 61 (1–2) (1996) 223–225.